ISSN 1063-7842, Technical Physics, 2024, Vol. 69, No. 6, pp. 1636–1645. © Pleiades Publishing, Ltd., 2024.
Russian Text © The Author(s), 2023, published in Zhurnal Tekhnicheskoi Fiziki, 2023, Vol. 93, No. 7, pp. 897–906.
English Text © Ioffe Institute, 2023.

# Influence of the Homobuffer Layer on the Morphology, Microstructure, and Hardness of Al/Si(111) Films

**A. A. Lomov[a,*], D. M. Zakharov[a], M. A. Tarasov[b], A. M. Chekushkin[b], A. A. Tatarintsev[a], D. A. Kiselev[c], T. S. Ilyina[c], and A. E. Seleznev[d]**

[a] *Valiev Institute of Physics and Technology, Russian Academy of Sciences, Moscow, 117218 Russia*
[b] *Kotelnikov Institute of Radio Engineering and Electronics, Russian Academy of Sciences, Moscow, 125009 Russia*
[c] *National University of Science and Technology "MISiS," Moscow, 119049 Russia*
[d] *Moscow State Technological University "STANKIN," Moscow, 127055 Russia*
**e-mail: lomov@ftian.ru*

Received April 12, 2023; revised April 12, 2023; accepted April 12, 2023

**Abstract**—The results of complementary studies of Al films grown by magnetron sputtering at room temperature are presented. The films were obtained on standard Si(111) substrates without and with a ~20 nm aluminum (homobuffer) layer preliminarily grown on their surface at 400°C. The interdependence of the morphology, microstructure, and hardness of Al films on the state of the substrate surface was studied by the HRXRR, XRD, SEM, EDS, AFM, and Nano Indenter (ASTM) methods. It is shown that the formation of homobuffer layers on the substrate surface makes it possible to control the structural and mechanical properties of thin aluminum films.

**Keywords:** aluminium, thin films, morphology, microstructure, XRD, SEM, and AFM, nanoindentation, magnetron sputtering

**DOI:** 10.1134/S1063784224060239

## 1. INTRODUCTION

Thin films of metals due to their properties are widely used in integrated circuits and devices of photonics, optoelectronics, micro- and superconducting electronics, quantum computers [1–5]. The composition of the films, as well as their microstructure, surface morphology and roughness of the interlayer boundaries basically determine the optical, electrical and magnetic properties of the structures created on their basis [6–10]. The production of monocrystalline metal films with atomically smooth surfaces is one of the priority directions for the development of growth technologies.

Traditionally, thermal evaporation and magnetron sputtering [7] are widely used for the formation of metal films. Most often, at the early stage of film formation, due to poor wettability of the substrate surface, insular grain growth occurs according to the Volmer–Weber model, in which the interatomic interaction between adatoms is greater than between the adatom and the substrate atom. As a result, the grown thin films are porous with a rough surface and high ohmic resistance [11, 12]. It should be noted that the roughness of the surface of the films is one of the principal barriers in the creation of effective Josephson tunnel junctions [13]. Thus, in case of a thermal evaporation of up to 20 nm thick aluminum films, the rms (root mean square) values of roughness and maximum surface deviations (peak to peak) were 2.3 and 23.3 nm [12], respectively. The transition to film growth by magnetron sputtering made it possible to obtain smoother surfaces with rms ~5 nm [14] on aluminum films with a thickness of 150 nm. The problem of surface roughness of films is closely related to the thermodynamic conditions of their growth. In the techniques mentioned earlier, films are formed polycrystalline with a certain texture, which can change as the film grows. This leads to the fact that the surface roughness of aluminum films during magnetron sputtering depends not only on the size of the crystallites, but also on the thickness of the films [15].

It was shown that single-crystal 100–3000 nm aluminum films can be formed by molecular beam epitaxy (MBE) on Si(111) [16], GaAs(001) [17], and $Al_2O_3$(0001) substrates [18]. In case of growing of the aluminum film on sapphire, the minimum rms value of the surface roughness was 0.6 nm at the growth temperature only at 750°C [18]. This result confirms the conclusions of earlier studies on the influence of growth conditions and atomic energies on the microstructure of films, the relationship of crystallite sizes with morphology and surface roughness.

The growth processes can be fundamentally changed during the formation of films by varying the

growth conditions. The use of the electron beam evaporation method showed that the transition from a stationary growth process to a two-stage one makes it possible to grow atomically smooth single crystal films of Ag/Si(111) [19]. Progress was achieved due to the formation of an island buffer Ag-layer at a high temperature on the substrate surface. The same approach is proposed to be used for growing films of aluminum and other metals [20].

Any growth process is affected by various interrelated factors that affect the formation of films in different ways. A limited number of methods are used in most works on this topic, which does not allow providing a complete picture of the relationship between the real structure and physical properties of films. This circumstance necessitates the use of a set of diagnostic methods.

This study is devoted to the structural characterization of Al films with a thickness of 150 nm on a Si(111) substrate grown by magnetron sputtering under the standard and two-stage mode of formation by a complex of complementary methods. The actual structure of the films (composition, surface morphology, microstructure) was determined by X-ray diffractometry at wide (XRD) and grazing incidence angles of (GIXRD), high-resolution X-ray reflectometry (HRXRR), quantitative X-ray microanalysis (EDS), scanning electron microscopy (SEM), scanning probe microscopy (AFM), mechanical characteristics of the films (hardness, Young's modulus) were obtained by nanoindentation (NI ASTM).

## 2. EXPERIMENT PROCEDURE

Aluminum films with a thickness of 150 nm were deposited on a Si(111) substrate with a thickness of 350 μm using a magnetron sputtering unit (Kurt J. Lesker Company Ltd., Germany) in a DC discharge mode and a power of 500 W. An aluminum target with a purity of 99.995% was used. Al films were deposited on the substrate both in one stage and in double stage mode. The film (conventional film – CF) was deposited in one stage mode in an argon atmosphere (pressure $4 \times 10^{-3}$ mbar) at a rate of 1.1 nm/s for a time of 138 s. In the double-stage mode, a homobuffer layer (HBL) of aluminum was pre-deposited on the substrate at 400°C at a rate of 0.2 nm/s with a thickness of ~20 nm. The aluminum was additionally deposited to the required film thickness at a rate of 1.1 nm/s at the second stage after cooling of the substrate with the HBL layer to room temperature (RT). CF and HBF films were grown at a temperature of 19–21°C.

The microstructure (phase composition, crystal lattice parameter $a$, thickness $L$, density, texture coefficient $P$, and size $g$ of crystallites) of Al films was studied using smartLAB X-ray diffractometer (9 kW, ITSoptics, Cu$K_\alpha$ radiation) in the geometry of a parallel beam. XRD ($2\theta/\omega$), GIXRD ($2\theta$, $\omega = 0.5°$, geometry off plain) diffractograms were recorded with a Soller slit installed in front of the detector window 0.114°). The mirror reflection curves $R(2\theta/\omega)$ and diffuse scattering cross sections $S(\omega, 2\theta = C_i)$ from surface roughness and submicron distortions were obtained in HRXRR mode using a Ge(220) slit monochromator with double reflection and an X-ray beam width 50 μm.

The morphology of the surface, the values of surface inhomogeneities and the composition of aluminum films were studied by SEM and EDS methods. The experiments were performed using Carl Zeiss Ultra 55 scanning electron microscope with an Oxford Instrument INCA X-act Xray energy dispersion spectrometer (EDS). The AFM method (Multifunctional Scanning Probe Microscope MFP3D Stand Alone (Oxford Instruments Asylum Research, USA)) with an NSG10 cantilever (Tipsnano, Tallinn, Estonia) was used to statistically describe the roughness and correlation coefficient of the film surface.

The hardness measurement $H$ and the calculation of the Young's modulus $E$ of the grown films were performed on the CB-500 Nanovea (USA) installation under the conditions of nanoindentation of a triangular Berkovich diamond pyramid.

## 3. RESULTS AND DISCUSSION

Analysis of the growth features of metal films shows that at high rates of deposition of atoms on a cold substrate, a large number of crystallization centers are formed on it. As a result, a polycrystalline film is formed on the substrate. In case of magnetron sputtering, the growth rate of the aluminum film in this study was determined by the peculiarities of the method and was equal to 1.1 nm/s, which is an order of magnitude higher than the growth rate in the methods of molecular beam epitaxy and electron beam evaporation. At the same time, when a film is formed its microstructure, morphology and roughness are affected by the substrate material, morphology and defects of the substrate surface, the presence of impurities [21, 22]. In most cases, a film with a microstructure consisting of predominantly (111) orientation of densely packed crystallites less than a micron in size in case magnetron sputtering of aluminum on a silicon substrate [23]. The orientation of microcrystallites and their size distribution determine the morphology of the surface. The roughness (RMS) of the film surface to a greater extent is determined by the distribution of crystallites in height than by the roughness of the surface of their growth faces, and also depends on the thickness of the film [14].

### *3.1. Electron Microscopy*

Images of chips of the studied Al/Si(111) samples with CF and HBF films grown without and with a homobuffer layer on a Si(111) substrate are shown in

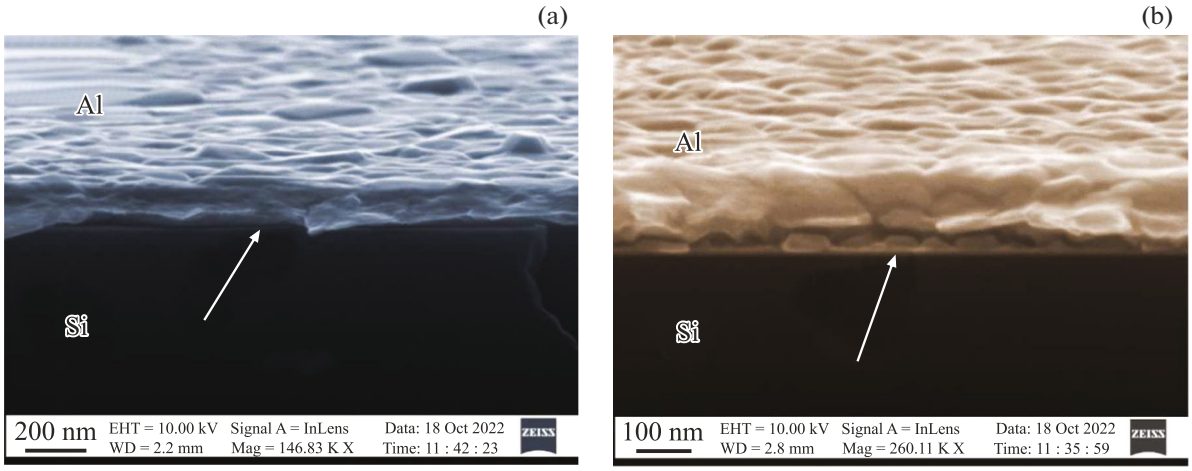


**Fig. 1.** SEM images of chips of magnetron films Al with a thickness of 150 nm grown at room temperature: in one stage mode (CF) (a) and with 400°C homobuffer layer (HBF) sputtered (b) on the substrate Si(111). The arrows show the boundary between the substrate and the film.

Fig. 1. It can be seen that, despite the formation of films under the same growth conditions (temperature, partial pressure, etc.), their surface morphology, the internal structure and mechanical properties are different.

For example, the lateral size of the "bumps" for the CF film produced by stationary deposition on the initial surface of the silicon wafer is ~1.5–2.5 times greater than this value for the HBF film grown on the homobuffer layer. The boundary between the CF and the substrate is quite sharp and solid, which is to be expected when deposited on a standard silicon substrate. At the same time, since the HBF was grown on a homobuffer layer consisting of ~30 nm aluminum islands, a loose transition layer ~20 nm with a large number of growth faces of nanocrystallites is observed at its boundary with the substrate. Attention is drawn to the difference in the image quality of the chips of these samples. If the background of the cleavage is blurred for the CF, then its structure clearly appears on the cleavage of the HBF. This result is confirmed by previous studies of the effect of the surface relief of substrates on the microstructure and mechanical properties of magnetron films [24].

### *3.2. X-ray Diffractometry*

The microstructure of grown aluminum CF and HBF can be analyzed on the basis of XRD and GIXRD diffractograms shown in Figs. 2a, 2b, respectively. The diffractograms in Fig. 2a obtained in the mode of standard $2\theta/\omega$ scanning reflect the scattering of X-rays on crystal planes parallel to the surface of the films. Diffraction peaks on GIXRD diffractograms (Fig. 2b) arise from crystal planes deflected from the film surface by the corresponding Bragg angles. The peaks observed on diffractograms (Fig. 2) from CF and HBF films at angles $2\theta = 38.5°$, 44.52°, 65.08°, 78.22°, and 82.48° correspond to reflections of 111, 200, 220, 311, 222 Al FCC lattice with constant $a = 0.405$ nm. The angular positions of the peaks from the Si(111) single crystal silicon substrate are outside the selected angular scanning area. Comparison of the number of peaks and the ratio of their intensities with the data (PDXL #01-080-5308) for a polycrystalline Al sample indicates that crystal films with different texture values along the plane (111) were obtained during the growth process.

CF film turns out to be the most textured. It can be seen that the main peaks on the diffractogram (Fig. 2a) from the film are reflections 111 and 222. Reflection 200 shows low intensity, while 220 and 311 are not observed. On the contrary, all possible peaks are recorded in the selected angular interval from a film having a homobuffer layer at the boundary with a silicon substrate, except for reflection 311. The microstructure of the HBF film is closer to polycrystalline. All possible diffraction reflections are visible on the GIXRD diffractograms (Fig. 2b) obtained at a grazing angle of incidence. The peak intensity ratios vary greatly both for one sample in different survey geometries and in comparison between samples. This is most strongly manifested for the CF film – there is a suppression of the reflection intensity 111 and the appearance of reflection 220. The reflection 311 is observed for both films under conditions of sliding radiation incidence. Reflection 311 from aluminum films is always observed in case of the study of polycrystalline samples. The aluminum films studied by us do not have crystallites with faces (311) parallel to the surface (Fig. 2a). Therefore, the reason for the appearance of reflection 311 may be related to diffraction on crystallites oriented with faces (111) parallel to the surface of the film (for reflection '311, the Bragg angle $\theta_B = 39.1°$

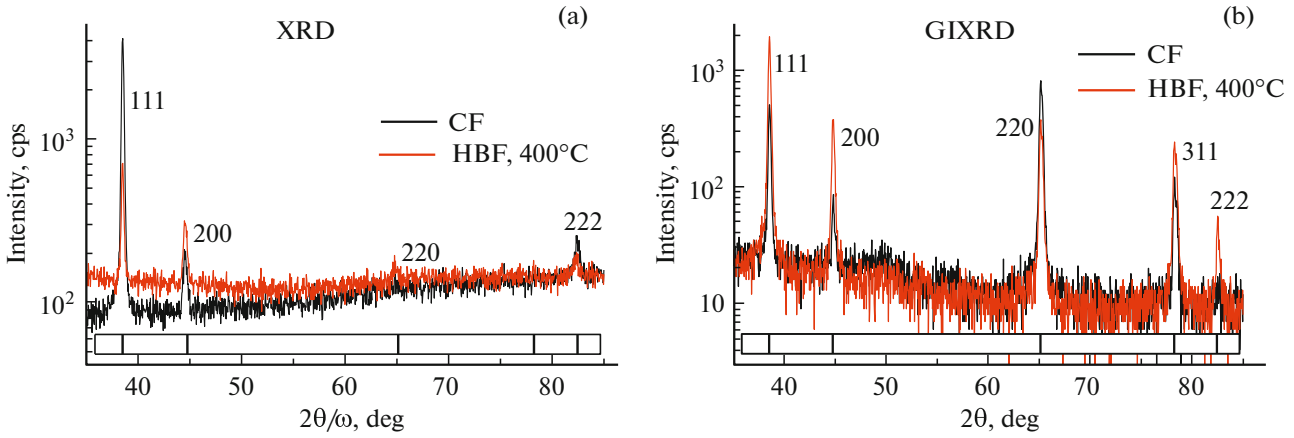


**Fig. 2.** Diffractograms from the studied Al/Si(111) films obtained in the symmetric 2θ/ω-scanning mode (a) and at a sliding angle of incidence φ = 0.5° of X-ray beam (b). Cu$K_\alpha$-radiation. For comparison, the black vertical lines under the curves show the positions of the diffraction peaks for the polycrystalline sample Al (PDXL #01-080-5308).

is greater than 29.5° – the angle between the planes (111) and (311)).

Analysis of the angular positions of the diffraction maxima shows within the instrumental error that undeformed ($\leq 3 \times 10^{-4}$) crystalline films were obtained in both growth modes. The ratio of the intensities of the corresponding reflections indicates the presence of a pronounced texture in the CF film (111), which can be seen from comparison with the data for a polycrystalline sample. The aluminum film grown with a homobuffer layer at 400°C is closer to a polycrystalline film. Qualitatively, this is manifested in a greater number of intense reflections compared to the CF film, and quantitatively (Table. 1) can be estimated using the value of the texture coefficient $P_{hkl}$ [25] for the selected reflection

$$P(h_ik_il_i) = \frac{I(h_ik_il_i)}{I_0(h_ik_il_i)}\left[\frac{1}{n}\sum_i^n \frac{I(h_ik_il_i)}{I_0(h_ik_il_i)}\right]^{-1}, \qquad (1)$$

where $h$, $k$, $l$ – Miller indices, $I$ and $I_0$ – integral reflection intensities for the studied sample and the diffraction data of the PDXL card. The intensities in the formula (1) are summed up with the substraction of the background for all observed reflections on the diffractogram. For an ideal polycrystalline sample, the value is $P_{hkl} \equiv 1$. Table 1 shows the texture coefficient for symmetrical 111 reflection from CF and HBF films ($P_{111}$), equal to 3.5 and 1.7, respectively. On the contrary, for the family of orthogonal (111) planes 110, the value of $P_{220} = 0$ and 0.4 for CF and HBF films, respectively. The presence of a pronounced texture in the studied films corresponds to the accepted model of [21] growth of the Al film at room temperature in the direction of [111].

The size of the crystallites in the studied films can be estimated from the analysis of the widths of diffraction peaks on diffractograms. For this purpose, various models of [26, 27] have been developed, taking into account the size, deformation and presence of packaging defects in crystallites. Analysis of the values of the half-widths of the peaks (Fig. 2) from various reflections 111, 200, 220 shows that, firstly, their half-widths $W$ do not correspond to the model of the classical powder – randomly arranged crystallites of the same size. In both cases, peaks 111, 220, and 311 reflections, taking into account the instrumental function and the corrections depending on the scattering angle, are already peaks 200 reflections. For both Al films, the half-width of $W_{111} \sim 0.2°$ is 1.5 times less than the value of $W_{200} \sim 0.3°$, which is a consequence of the presence of a bimodal particle distribution. According to the Zone Growth Model [6, 21], the formation of dense textured films with a columnar microstructure along the direction [111] was assumed in the work. The presence of reflection on diffractograms (Fig. 2) 200 indicates the presence of metastable crystallites in the Al film [28]. When metal films are formed under

**Table 1.** Characteristics of Al/Si(111) films with a thickness of 150 nm grown by magnetron sputtering

| Samples | $P_{hkl}$, (XRD) | | RMS, nm (AFM) | $R_{max}$, nm (AFM) | ξ, nm (AFM) | $H$, GPa (NI) | $H$, GPa (Ni) |
|---|---|---|---|---|---|---|---|
| | (111) | (220) | | | | | |
| CF | 3.5(2)* | 0 | 6.3 | 35 | 105(2) | 5.4(5) | 1.1(1) |
| HBF | 1.7(2) | 0.4(1) | 6.5 | 10 | 57(1) | 16(1) | Al/Si sub |

**Table 2.** Crystallite size $D$ for Al/Si(111) films according to Xray diffractometry data in symmetric (XRD) and sliding (GIXRD) geometry

| Film | XRD | | | | GIXRD | | | |
|---|---|---|---|---|---|---|---|---|
| | $D_{111}$, nm | $D_{200}$, nm | $D_{220}$, nm | $D_{311}$, nm | $D_{111}$, nm | $D_{200}$, nm | $D_{220}$, nm | $D_{311}$, nm |
| CF | 50(5) | 30(5) | – | – | 49(5) | 36(5) | 53(5) | 51(5) |
| HBF | 51(5) | 30(5) | 56(5) | – | 50(5) | 35(5) | 58(5) | 59(5) |

equilibrium conditions, the state when the surface of the crystallite coincides with the planes having a minimum energy of γ activation of the surface is energetically advantageous. Calculations for [29] aluminum having a FCC lattice, the energies of γ in the model of broken bonds give values of 0.9108 and 1.0438, respectively, for planes (111) and (100). This result explains the formation of texture (111) in aluminum films and confirms the well-known Bravais law of crystals faces with planes with high reticular density and the presented models of transformation of the shape of nanocrystallites with a FCC lattice depending on the ratio $R$ of the growth rates of the plane (1 0 0) to (1 1 1) [26].

Table 2 shows the sizes of crystallites calculated for various reflections in symmetric and sliding geometry based on the formula Scherrer [26, 27]:

$$D = \frac{K\lambda}{W(2\theta)\cos(\theta)}, \quad (2)$$

where $W(2\theta)$ – peak width at half height, λ – radiation wavelength, $K \sim 0.94$. Values $W(2\theta)$ for calculations using the formula (2) were reconstructed from the experimental values of the half-widths of the peaks, taking into account their convolution with the instrumental function, the shape of which corresponded to the diffraction peak 111 of reflection from the silicon substrate.

The analysis of the results listed in Table and values of texture coefficients *Phkl* (Table 1) shows that the difference in the microstructure (Fig. 2) of CF and HBF films is determined by the distribution of crystallites by their shape and orientation in the film, and not by their average size. As a result, aluminum films grown under the same growth conditions on Si substrates without and with a homobuffer layer have different morphology and surface roughness, as well as hardness (Table 1).

The results of the study of distortions and roughness of their surface by high-resolution X-ray reflectometry correlate with the features of the microstructure of films [27, 30]. Figure 3a shows experimental curves of specular reflection from CF and HBF films, as well as a model curve [31] calculated for an aluminum film with a thickness of $L = 150$ nm with a density of $\rho = 2.7$ g/cm$^3$ and radiation with $\lambda = 0.15406$ nm. It is clearly seen that the main features of the curves: the angle of total external reflection $\theta_c \sim \sqrt{\rho}$ and the oscillation period $\Delta 2\theta \approx \lambda/L$ [30] coincide. Consequently, CF and HBF aluminum films of equal thickness of 150(1) nm were formed with the selected growth mode. However, the specular reflectance on the "tails" reflection curves (Fig. 3a) is noticeably different. Firstly, the intensity of the mirror reflection of the HBF film at angles $\theta > \theta_c$ decreases more sharply compared to the film grown in a single-stage process. The amplitudes of the thickness oscillations (Kiessing frienges) for the HBF sample are less pronounced and fade faster. The behavior of the reflectance from the samples observed in Fig. 3a is attributable to the difference in morphology, surface roughness and internal transition layers of film–substrate. Any inhomogeneities of the electron density at both boundaries of the film and the transition layers will lead to the appearance of diffuse scattering and a decrease in the intensity of the coherent mirror component. The analysis of diffuse scattering and the restoration of the parameters of the roughness of the boundaries in multilayer structures is a separate task [32, 33]. However, the method of ω-scanning of the diffuse scattering can characterize distortions, surface relief and interlayer boundaries of the layer [30, 32–34].

Figure 3b shows the cross sections of diffuse scattering of X-rays at sliding angles of incidence from the studied films. The curves were obtained by ω-scanning the sample at a fixed $2\theta_i$ position of the detector with a narrow slit. There are three maxima on the curves: *1* and *2* – the so-called peaks or Yoneda wings [30, 32] and a narrow peak *3* at the site of the mirror reflection at $2\theta = 0.8°$. The peak *1* is caused by diffuse scattering on the relief of the input surface of the film. The diffuse scattering from the film surface and from the inhomogeneity of the electron density in the transition layer of the film-substrate contributes to the peak intensity *2*. A good match of peak intensity values *1* (Fig. 3b) for CF and HBF films and the number of oscillations on the curves (Fig. 3a) shows that the RMS values of the surface roughness of the films are close, but additional studies and the construction of the PSD [33] spectral density function are needed, taking into account the diffuse scattering from the transition layer of the film-substrate. The appearance of this additional diffuse scattering at the boundary with the substrate for a sample with a HBF homobuffer layer leads to a significant increase in the intensity of the second Yoneda peak (Fig. 3b). Intense diffuse scattering for the HBF sample explains the lower

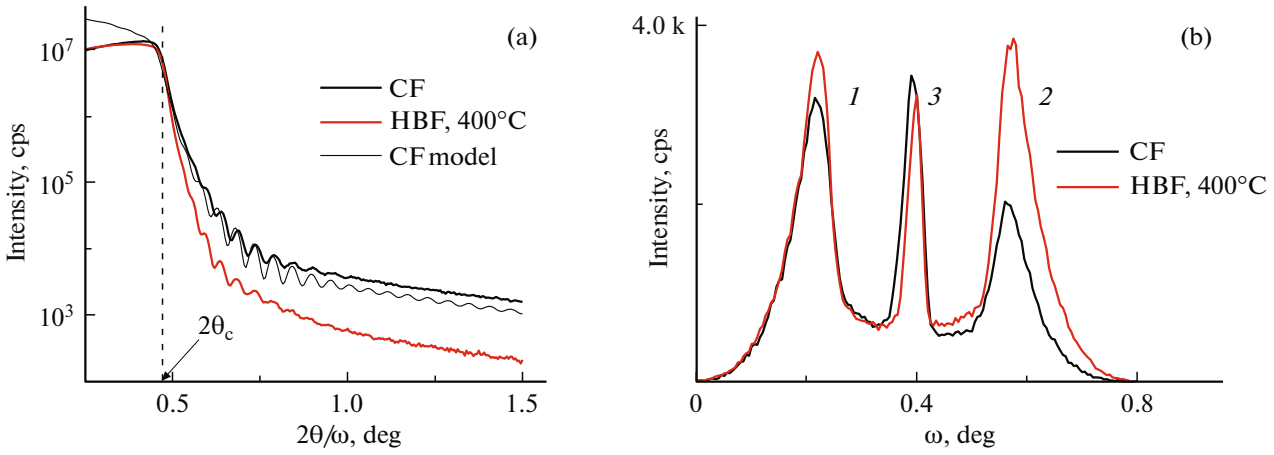


**Fig. 3.** X-ray mirror reflection curves from the studied CF and HBF aluminum films with a thickness of 150 nm (a) and ω are diffuse scattering cross sections for $2\theta = 0.8°$ (b). $\theta_c = 0.2356°$ [31], *1* and *2* – peaks of Yoneda wings, *3* – peak at mirror reflection angle.

intensity of the "tail" of the specular reflection curve (Fig. 3a).

As already noted, coherent scattering forms a specular reflection at $\omega = 2\theta/2$, and its intensity away from the critical angle can be calculated, for example, in the Born approximation for fine surface roughness, when the contribution of diffuse scattering is insignificant. The diffuse scattering [34] will make the main contribution to the scattering intensity in the mirror direction if there are large electron density inhomogeneities (distortions and relief) at the boundaries of the layers (surface). This case is observed in Fig. 3a, on which "tails" reflection curves smoothly fall off at large angles. Calculating the peak intensity *3* and extracting the parameters of the layer model becomes a non-trivial task. However, the presented result shows that the HRXRR technique opens up wide possibilities for nondestructive testing of homobuffer layers.

### *3.3. AFM*

Figures 4a, 4b shows images of local surface areas of CF and HBF samples obtained by atomic-force microscopy (AFM). Rare large hills are observed on the surface of the CF sample in addition to numerous bumps (Fig. 4a). The surface relief of the HBF sample is more uniform with randomly located bumps of approximately equal size. Attention is drawn to both qualitative and quantitative differences in the lateral dimensions and heights of the observed surface distortions, despite the same (with the exception of the homobuffer layer) growth conditions of aluminum films. Numerous bumps on the surface of the CF film (Fig. 4a) are ~2 times wider than the bumps of the HBF film (Fig. 4b). At the same time, the average heights of the bumps and their amplitude values for the studied samples practically coincide. The RMS calculation of the roughness heights (bumps) of the surface of the films was performed using Gwiddion-2.60 software based on several surface sections without taking into account large distortions (hills) and is presented in Table 1. During the analysis of the surface roughness of CF and HBF samples the RMS value steadily showed a lower value: 6.3 and 6.5 nm, respectively. The amplitude of the Rmax hills on the CF sample surface reaches 35 nm versus 10 nm for the HBF sample surface with a homobuffer layer.

When the relief of the film surface is compared, for example, with its electrophysical and optical characteristics, the lateral size of inhomogeneities is of great importance. It can be quantified through the parameters of the autocorrelation function $C(r)$ [35]:

$$C(r) = \sigma^2 \exp\left[-\left(\frac{r}{\xi}\right)^{2h}\right] + (1-\sigma^2)\exp\left[-\frac{r}{r_c}\right]\cos\left(\frac{\pi r}{a}\right), \quad (3)$$

where σ – normalization coefficient, $r$ – polar coordinate, $r_c$ – long-range correlation length in the presence of periodicity $a$ analyzed objects (hillocks), ξ – the correlation length of the nearest objects on the surface, $h = 0 - 1$ and characterizes the blurriness of the boundary between them.

The images of the surface of the films were processed using wsxm.eu (WSxM v5.0 Develop 10.2). Figure 4e shows the best fit of $C(r)$ for its numerical values, recovered based on image processing of the sample surface. The values of the parameter ξ – the short-range correlation lengths for "bumps" or "depressions" on the surface – were equal to 104.6(3) nm at $h = 0.83$ and 57.6(4) nm at $h = 1.03$ for CF and HBF, respectively (Table 1). A comparative analysis of the results of AFM studies of CF and HBF samples shows that the aluminum film grown on the homobuf-

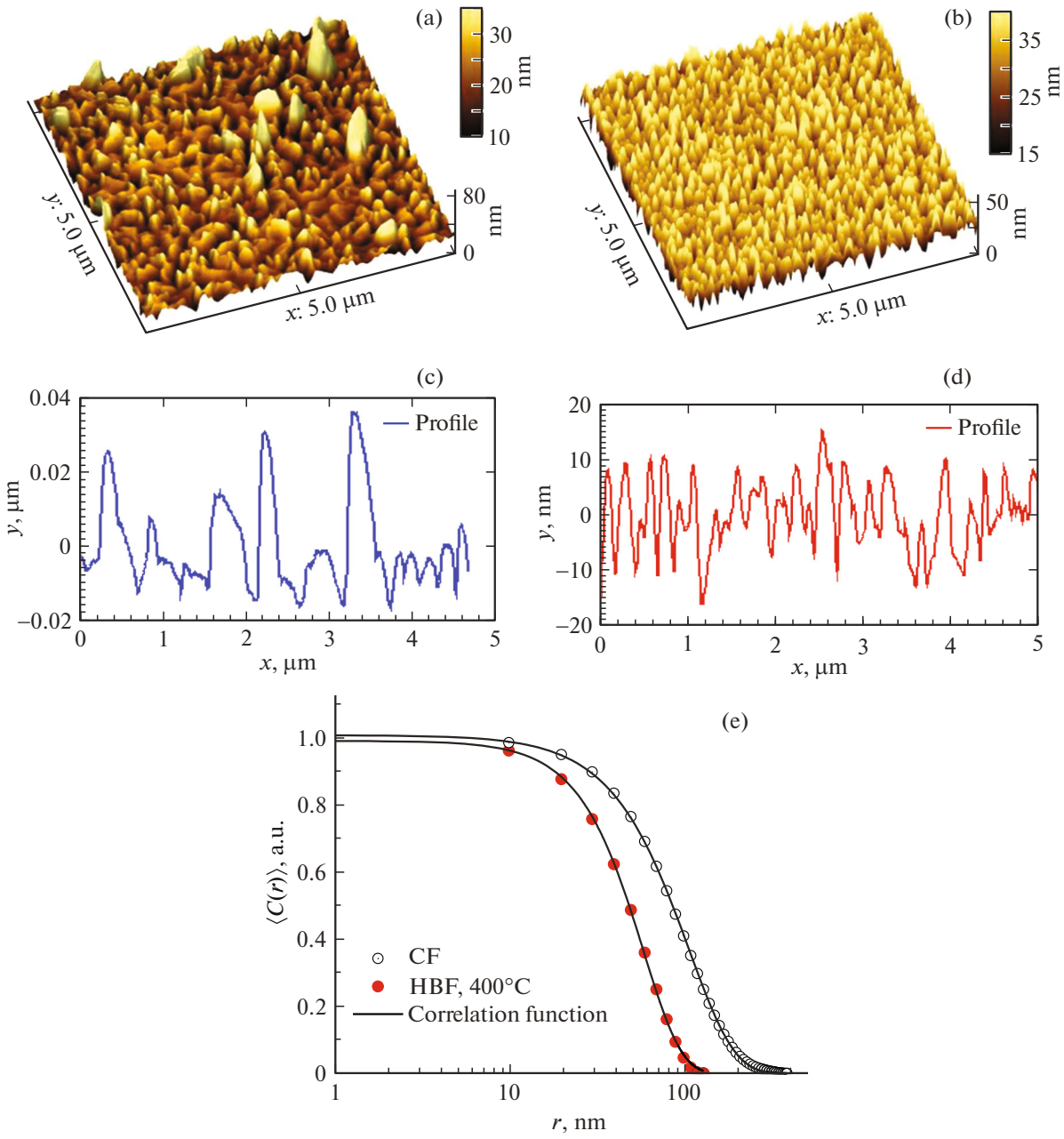


**Fig. 4.** Three-dimensional AFM images of films: CF (a), with a homobuffer layer HBL (b); profiles of films CF (c) and HBL (d); correlation function for both films (e).

fer layer has a more homogeneous, less rough and with a finer relief surface.

### *3.4. X-Ray Microanalysis*

The aluminum films on a silicon substrate were studied using energy dispersion spectrometry (EDS). An electron probe with an energy of 20 keV and a diameter of 1 nm was used. The probe current was calibrated using a cobalt sample before the start of the study. During the measurement process, the deviation of the probe current from the nominal value did not exceed 1%. The secondary X-ray signal was recorded during scanning a square area with a characteristic side size of 100 μm using an electron probe. The geometry and spectra recording conditions for the studied samples were identical.

Figure 5 shows the EDS spectra from CF and HBF samples. The peaks of the characteristic (Kα-line, $E$ = 1.48 keV) X-ray radiation from both Al films, as well as from the Si substrate (Kα-line, $E$ = 1.74 keV). Additional peaks from impurities present in the films corre-

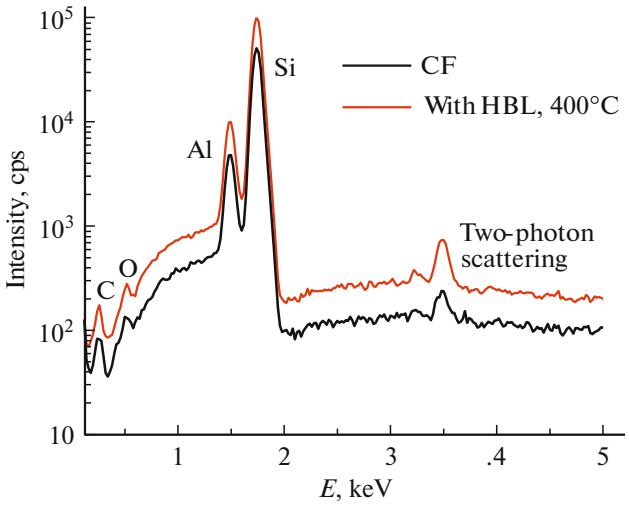


**Fig. 5.** EDS spectra from Al/Si(111) films acquired in various growth modes.

spond to Kα-lines of carbon (280 eV) and oxygen (530 eV). Peaks with doubled energy Kα-lines of aluminum and silicon are visible on the X-ray spectra as artifacts. The presence of such peaks is caused by the high intensity of the signal recorded by the spectrometer and is associated with the almost simultaneous registration of two X-ray quanta by a semiconductor detector. It should be noted that the intensity of both deceleration and characteristic X-rays in each energy window from the HBF sample is almost twice as high as for the CF sample on the presented EDS spectra acquired under the same conditions.

The results of quantitative X-ray microanalysis for two samples of CF and HBF films averaged over 5 points are listed in Table 3. The results show that the composition of Al/Si(111) films grown under different growth modes is the same within the limits of heterogeneity of composition and measurement error.

The analysis of the signal intensity ratio on the spectra (Fig. 5) shows that the intensity of both deceleration and characteristic X-rays in each energy window from the HBF sample is almost twice as high as from the CF sample obtained in a single-stage growth mode. The difference in the magnitude of the EDS signal from CF and HBF films may be related to the effective surface size determined by the roughness and relief parameters. The observed SEM images of the surface in Fig. 1 allow estimating the lateral dimensions of the main bumps as 150–250 and 40–70 nm for CF and HBF samples, respectively. Rare bumps with a lateral size of more than 250 nm and a height of ~60 nm are also visible (Fig. 1a). The decrease in the lateral size of the bumps for the HBF film is confirmed by AFM data (Fig. 4) and correlates with an increase of the EDS signal. The question of the effect of surface roughness on the output of fluorescent X-rays was investigated and described in [36]. This paper recommends to reduce the roughness of the studied surface to a value less than 50–100 nm for X-ray microanalysis. However, the effect of heights and lateral dimensions of surface distortions on the X-ray output was not specified.

### *3.5. Nanoindentation*

The above results of the study of the effect of the homobuffer layer on the morphology and microstructure of aluminum films were compared with changes in their hardness $H$ and Young's modulus $E$, determined by the nanoindentation technique [37, 38]. Figure 6 shows the direct (loaded) and inverse (unloaded) dependences of the applied load $P$ on the penetration depth of the indenter in the mode of continuous stiffness measurement $S = dP/dh$ on the studied films CF and HBF. The measurements of the mechanical properties of nanoscale films are associated with the hazard of penetration of the indenter into the substrate area. Preliminary recordings of the loading curves showed that the load range should not exceed 5 mN for the studied films. The spread of hardness values $H = P_{max}/A$ ($A = 24.5h_c^2$, $h_c = h_{max} - 3P_{max}/4S$ [38]), reconstructed using Nanovea software (http://nanovea.com/NanoIndentationTester), did not exceed 15% in the specified load range $P$.

For convenience of comparing the load curves of the immersion of the $h$ indenter on the magnitude of the applied load, they are combined at $P_{unload}(0) = 0$ (Fig. 6). It is clear that the stiffness $S$ of the aluminum film grown on the homobuffer layer increases with depth more sharply than for the film formed on the original silicon substrate. The average hardness (Table. 1) and $E$ for CF and HBF samples, determined based on 5 measurements at different points of their surface, is equal to: $H = 5.4$ GPa, $E \sim 55$ GPa and $H = 16$ GPa, $E \sim 100$ GPa respectively. The Poisson's ratio ν was assumed to be 0.34 for the calculations [39]. The hardness of the magnetron 1000 nm Al film on the Si substrate at the immersion depth of the nanoindent $h < 100$ nm was $H = 1.1–1.2$ GPa, and $E \sim 90$ GPa [40]. In our opinion, the coincidence of the hardness of the

**Table 3.** Results of quantitative X-ray microanalysis (EDS)

| Sample | Atomic % C | Atomic % O | Atomic % Al | Atomic % Si |
|---|---|---|---|---|
| CF | 11.8 | 1.3 | 5.5 | 81.3 |
| HBF | 10.9 | 1.5 | 5.9 | 81.7 |

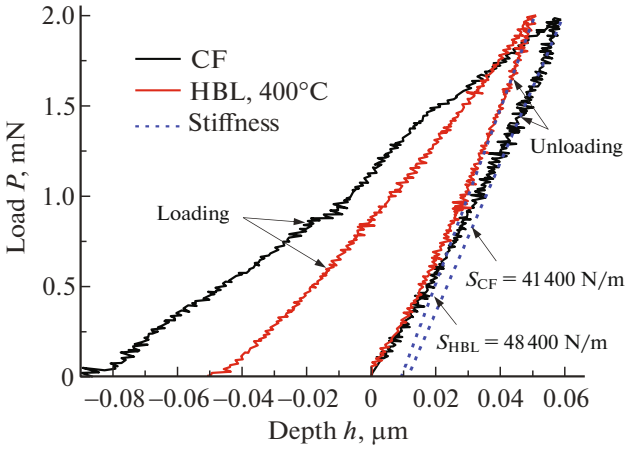


**Fig. 6.** Direct and inverse dependences of the applied load on the depth of penetration of the Berkovich nanoindenter into the films CF and HBF.

studied Al-films and the data of [40] without taking into account their morphology and microstructure can be considered to be good. Indeed, the ratio of yield strength to elastic modulus is small for Al [39]. This can lead to deformation hardening due to the indentation of the material and a change in the area around the nanoindentor. Modeling under elastic-plastic conditions shows [41] the effect of deformation on the shape of the boundaries of aluminum crystallites with dimensions 20–40 nm and on the behavior of polycrystalline microstructure. Since the aluminum film grown on the homobuffer layer is less textured (Table 1) it has a more chaotic arrangement of crystallites and, naturally, their boundaries, its hardness turned out to be higher. This result conforms with the model of film hardening through the impact of grain boundaries on its hardness [42].

## CONCLUSIONS

This paper provides the results of the study of aluminum films with a thickness of 150 nm grown by magnetron sputtering on standard Si(111) silicon substrates without and with a homobuffer 20 nm layer on the surface based on a set of complementary methods. The study was conducted using X-ray diffractometry methods in symmetric and sliding geometry, X-ray reflectometry, scanning electron and atomic-force microscopy, nanoindetization. The main parameters of the morphology and microstructure of the films are determined and it is shown that the introduction of a homobuffer layer leads to: a decrease of the (111) texture of the film without changing the size of the (111) crystallites the formation of regular roughness with RMS = 6.5 nm and a correlation length of 60 nm; an up to three-fold increase of the nanohardness of the film. The impact of the homobuffer layer on the ω-curves of X-ray reflectometry is shown and it is proposed to use it to characterize homobuffer layers in the process of their transformation. And, finally, the possibility of controlling the physical properties of an aluminum film by forming a homobuffer layer on a silicon substrate is shown.

## FUNDING

The work was performed under of the State Assignment of the Valiev Institute of Physics and Technology of Russian Academy of Sciences of the Ministry of Education and Science of the Russian Federation on the topic FAN2022-0019. The development and study of samples was performed in Kotelnikov Institute of Radioengineering and Electronics and was financed by the grant from the Russian Scientific Foundation RSCF 23-79-00022, https://rscf.ru/project/23-79-00022/. The experimental samples were produced under the state assignment in Kotelnikov Institute of Radioengineering and Electronics of the Russian Academy of Sciences. The equipment of the Unique scientific unit 352529 “Cryointegral”, supported by a grant from the Ministry of Science and Higher Education of the Russian Federation under the agreement 075-15-2021-667, was used for fabrication of samples.

## CONFLICT OF INTEREST

The authors declare that they have no conflict of interest.

## REFERENCES

1. G. Hass, M. H. Francombe, J. L. Vossen. *Physics of Thin FilmsResearch and Development* (Academic Press, NY., USA, 1982)
2. K. Barmak, K. Coffey. Metallic Films for Electronic. *Optical and Magnetic Applications* (Woodhead Publishing, Cambridge, UK, 2013)
3. M. A. Tarasov, L. S. Kuzmin, V. S. Edelman, S. Mahashabde, P. de Bernardis. IEEE Transactions on Applied Superconductivity, **21** (6), 3635 (2011). https://doi.org/10.1109/TASC.2011.2169793
4. N. Samkharadze, G. Zheng, N. Kalhor, D. Brousse, A. Sammak, U. C. Mendes, A. Blais, G. Scappucci, L. M. K. Vandersypen. Science, **359** (6380), 1123 (2018). https://doi.org/10.1126/science.aar4054
5. M. C. Rao, M. S. Shekhawat. Intern. J. Modern Physics: Conf. Series, **22**, 576 (2013). https://doi.org/10.1142/S2010194513010696
6. N. Kaiser. Appl. Opt., **41** (16), 3053 (2002).
7. M. Ohring. *The Material Science of Thin Films* (Academic Press, San Diego, Calif., USA, 1992)
8. J. Venables. *Introduction to Surfaces and Thin Film Processes* (Cambridge U. Press, Cambridge, UK, 2000)
9. D. Sibanda, S. T. Oyinbo, T. -C. Jen, A. I. Ibitoye. Processes, **10** (6), 1184 (2022). https://doi.org/10.3390/pr10061184
10. R. Eason. *Pulse Layer Deposition: Application-Led Growth of Functional Materials.* (John Wiley & Sons,

Inc., Hoboken, New Jersey, 2007), https://doi.org/10.1002/0470052120

11. I. V. Antonets, L. N. Kotov, S. V. Nekipelov, E. A. Golubev. ZhTF, **74**(3), 24 (2004) (in Russian).
12. M. A. Tarasov, L. S. Kuzmin, N. S. Kaurova. Instrum. Exp. Tech., **52**, 877 (2009). https://doi.org/10.1134/S0020441209060220
13. V. V. Roddatis, U. Hubner, B. I. Ivanov, E. Il'ichev, H.-G. Meyer, A. L. Vasiliev. J. Appl. Phys., **110**, 123903 (2011). https://doi.org/10.1063/1.3670003
14. M. Tarasov, A. Gunbina, M. Fominsky, A. Chekushkin, V. Vdovin, V. Koshelets, E. Sohina, A. Kalaboukhov, V. Edelman. Electronics, **10** (23), 2894 (2021). https://doi.org/10.3390/electronics10232894
15. U. Barajas-Valdes, O. M. Suarez. Crystals, **11** (5), 492 (2021). https://doi.org/10.3390/cryst11050492
16. A. W. Fortuin, P. F. A. Alkemade, A. H. Verbruggen, A. J. Steinfort, H. Zandbergen, S. Radelaar. Surf. Sci., **366** (2), 285 (1996). https://doi.org/10.1016/0039-6028(96)00824-2
17. A. Y. Cho, P. D. Dernier. J. Appl. Phys., **49** (6), 3328 (1978). https://doi.org/10.1063/1.325286
18. W. Wang, W. Yang, Z. Liu, Yu. Lin, S. Zhou, H. Qian, H. Wang, Z. Lin, G. Li. Cryst. Eng. Comm., **16** (33), 7626 (2014). https://doi.org/10.1039/c4ce01076k
19. I. A. Rodionov, A. S. Baburin, A. R. Gabidullin S. S. Maklakov, S. Peters, I. A. Ryzhikov, A. V. Andriyash. Scientif. Reports, **9**, 12232 (2019) https://doi.org/10.1038/s41598-019-48508-3
20. I. A. Rodionov, A. S. Baburin, I. A. Ryzhikov. Patent US 2021/0071292 A1 (2021).
21. F. M. Mwema, O. P. Oladijo, S. A. Akinlabi, E. T. Akinlabi. J. Alloys Compd., **747**, 306 (2018). https://doi.org/10.1016/j.jallcom.2018.03.006
22. M. Adamik, P. B. Barna, I. Tomov. Thin Solid Films, **317**, 64 (1998).
23. J. F. Smith, F. T. Zold, W. Class. Thin Solid Films, **96**, 291 (1982). https://doi.org/10.1016/0040-6090(82)90513-2
24. J. Lin, J. J. Moore, W. D. Sproul, S. L. Lee, J. Wang. IEEE Transac. Plasma Sci., **38** (11), 3071 (2010). https://doi.org/10.1109/TPS.2010.2068316
25. M. Kumar, A. Kumar, A. C. Abhyankar. ACS Appl. Mater. Interfaces, **7** (6), 3571 (2015). https://doi.org/10.1021/am507397z
26. S. C. Tjong, H. Chen. Mater. Sci. Engineer., R **45**, 1 (2004). https://doi.org/10.1016/j.mser.2004.07.001
27. M. Birkholz. *Thin Film Analysis by X-ray Scattering.* (Weinheim: Wiley–VCH, 2006), https://doi.org/10.1002/3527607595
28. B. M. McSkimming, A. Alexander, M. H. Samuels. J. Vac. Sci. Technol. A, **35**, 021401 (2017). https://doi.org/10.1116/1.4971200
29. S. G. Wang, E. K. Tian, C. W. Lung. J. Phys. Chem. Solids, **61**, 1295 (2000). https://doi.org/10.1016/S0022-3697(99)00415-1
30. K. Stoev, K. Sakurai. The Rigaku J., **14** (2), 22 (1997).
31. S. A. Stepanov. X-ray Server, (1997). https://x-server.gmca.aps.anl.gov.
32. V. Holy, U. Pietsch, T. Baumbach. *High- Resolution X-ray Scattering from Thin Films and Multilayers* (Springer-Verlag, Berlin, Heidelberg, 1999)
33. I. V. Kozhevnikov, A. V. Buzmakov, F. Siewert, K. Tiedtke, M. Stormer, L. Samoylova, H. Sinn. J. Synchrotron Rad., **23**, 78 (2016). https://doi.org/10.1107/S160057751502202X
34. V. I. Punegov, Ya. I. Nesterets, S. V. Mytnichenko, N. V. Kovalenko, V. A. Chernov. Poverhnost. X-ray, Synchrotron and Neutron investigation, **1**, 58 (2003). (russian)
35. V. V. Shvartsman, A. L. Kholkin. J. Appl. Phys., **101** (6), 064108 (2007). https://doi.org/10.1063/1.2713084
36. J. I. Goldstein, D. E. Newbury, J. R. Michael, N. W. M. Ritchie, J. H. J. Scott, D. C. Joy. *Scanning Electron Microscopy and XRay Microanalysis* (Springer, NY., USA, 2018), https://doi.org/10.1007/978-1-4939-6676-9
37. W. C. Oliver, G. M. Pharr. J. Mater. Res., **7** (6), 1564 (1992). https://doi.org/10.1557/JMR.1992.1564
38. M. J. Schneider, M. S. Chatterjee. *Introduction to Surface Hardening of Steels, ASM Handbook, Volume 4A*. (ASM International, USA, 2013), https://doi.org/10.31399/asm.hb.v04a.a0005771
39. X. Li, B. Bhushan. Mater. Character., **48**, 11 (2002). https://doi.org/10.1016/S1044-5803(02)00192-4
40. G. V. Samsonov. *Handbook of the Physicochemical Properties of the Elements* (IFI-Plenum, NY., USA, 1968), https://doi.org/10.1007/978-1-4684-6066-7
41. A. Prakash, D. Weygand, E. Bitzek. Intern. J. Plasticity, **97**, 107 (2017). https://doi.org/10.1016/j.ijplas.2017.05.011
42. E. N. Hahn, M. A. Meyers. Mater. Sci. Engineer.: A, **646**, 101 (2015). https://doi.org/10.1016/j.msea.2015.07.075